PCCP

PAPER

View Article Online
View Journal | View Issue

Cite this: *Phys. Chem. Chem. Phys.*, 2024, **26**, 11597

Chemisorption of silicon tetrachloride on silicon nitride: a density functional theory study†

Tanzia Chowdhury, [a] Khabib Khumaini, [ab] Romel Hidayat, [ac] Hye-Lee Kim [ac] and Won-Jun Lee *[ac]

Received 28th November 2023,
Accepted 15th March 2024

DOI: 10.1039/d3cp05799b

rsc.li/pccp

We studied the chemisorption of silicon tetrachloride ($SiCl_4$) on the NH_2/NH-terminated silicon nitride slab model using density functional theory (DFT) for atomic layer deposition (ALD) of silicon nitride. Initially, two reaction pathways were compared, forming HCl or $NH_3^+Cl^-$ as a byproduct. The $NH_3^+Cl^-$ complex formation was more exothermic than the HCl formation, with an activation energy of 0.26 eV. The $-NH_2$* reaction sites are restored by desorption of HCl from the $NH_3^+Cl^-$ complexes at elevated temperatures of 205 °C or higher. Next, three sequential ligand exchange reactions forming Si–N bonds were modeled and simulated. The reaction energies became progressively less exothermic as the reaction progressed, from −1.31 eV to −0.30 eV to 0.98 eV, due to the stretching of Si–N bonds and the distortion of the N–Si–N bond angles. Also, the activation energies for the second and third reactions were 2.17 eV and 1.55 eV, respectively, significantly higher than the 0.26 eV of the first reaction, mainly due to the additional dissociation of the N–H bond. The third Si–N bond formation is unfavorable due to the endothermic reaction and higher activation energy. Therefore, the chemisorbed species would be $-SiCl_2$* when the surface is exposed to $SiCl_4$.

Introduction

As the integration density of semiconductor devices continues to increase, advanced thin film deposition techniques such as atomic layer deposition (ALD) are being adopted in semiconductor manufacturing. ALD is an atomic layer-by-layer growth technique in which the substrate surface is alternately exposed to a precursor and a co-reactant. The self-limiting nature of ALD provides precise process control over material thickness, composition, and conformality in high aspect ratio (HAR) patterns. ALD of silicon nitride is used for various applications such as gate spacers[1] and diffusion barriers[2] in complementary metal-oxide-semiconductor (CMOS) devices and charge trapping[3] and sacrificial layers[3] in three-dimensional vertical NAND flash memory devices.

The ALD process of silicon nitride can be achieved by thermal ALD or plasma-enhanced ALD (PEALD). Although various types of silicon precursors, such as chlorosilanes,[4–6] aminosilanes,[7,8] silylamines,[9,10] cyclosilazanes,[11,12] and silanes,[4,13] have been investigated in PEALD, only chlorosilane-type silicon precursors have been studied in thermal ALD processes, such as silicon tetrachloride ($SiCl_4$),[14,15] dichlorosilane (DCS, SiH_2Cl_2),[15] hexachlorodisilane (HCDS, Si_2Cl_6),[16] and octachlorotrisilane (OCTS, Si_3Cl_8).[17] Ammonia (NH_3)[14,15,17,18] or hydrazine (N_2H_4)[16,19] was used as the coreactant for thermal ALD.

The reaction mechanism of thermal silicon nitride ALD using $SiCl_4$ was investigated by *in situ* FTIR spectroscopy.[14] $SiCl_4$ reacts with the $-NH_x$ surface site to form $-NSiCl_x$ with an HCl byproduct, and then NH_3 reacts with $-NSiCl_x$ to restore $-NH_x$, resulting in the growth of silicon nitride film. Density functional theory (DFT) calculations were used to study the reaction mechanism of the ALD process of silicon nitride.[20–26] The surface reaction of bis(diethylamino)silane or bis(*tert*-butylamino)silane was studied on the β-Si_3N_4 (0001) slab model.[24] The surface reaction of $SiCl_4$, SiH_2Cl_2, Si_2Cl_6, or Si_3Cl_8 to form a Si–N bond was also studied on the NH/NH_2-terminated β-Si_3N_4 (0001) slab model.[25] Different silicon tetrahalides were compared by simulating the sequential ligand exchange reactions forming multiple Si–N bonds using the NH_2-terminated Si cluster model.[27]

The above DFT studies assumed the formation of an HCl molecule as a reaction byproduct. However, Hartmann *et al.*[26] studied the surface reaction of SiH_2Cl_2 and suggested that the H from the $-NH_2$ could migrate to another $-NH_2$ site to form an $NH_3^+Cl^-$ complex instead of directly forming a gaseous HCl byproduct, resulting in a lower system energy. The formation of the $NH_3^+Cl^-$ complex has also been demonstrated by *in situ* FTIR and XPS analyses.[28] To date, no comparative study has

[a] *Department of Nanotechnology and Advanced Materials Engineering, Sejong University, Seoul, 05006, Republic of Korea*
[b] *Department of Chemistry, Universitas Pertamina, Jakarta 12220, Indonesia*
[c] *Metal-organic Compounds Materials Research Center, Sejong University, Seoul, 05006, Republic of Korea. E-mail: wjlee@sejong.ac.kr*

† Electronic supplementary information (ESI) available. See DOI: https://doi.org/10.1039/d3cp05799b

been performed between the direct formation of an HCl molecule and the formation of an $NH_3^+Cl^-$ complex on the surface.

In this study, the chemisorption mechanism of a $SiCl_4$ molecule on a silicon nitride surface terminated with NH_2 and NH groups was investigated. $SiCl_4$ was chosen as the precursor to be investigated because it is the most basic chlorosilane molecule. First, the formation of the $NH_3^+Cl^-$ complex was compared to the formation of HCl. The desorption of HCl from the $NH_3^+Cl^-$ complex, resulting in the restoration of the original $SiNH_2^*$ site, where the asterisk (*) indicates the surface species, was also studied. Finally, the sequential ligand exchange reactions forming Si–N bonds were modeled and simulated. The reaction and activation energies were obtained to suggest the end product of the chemisorption of $SiCl_4$.

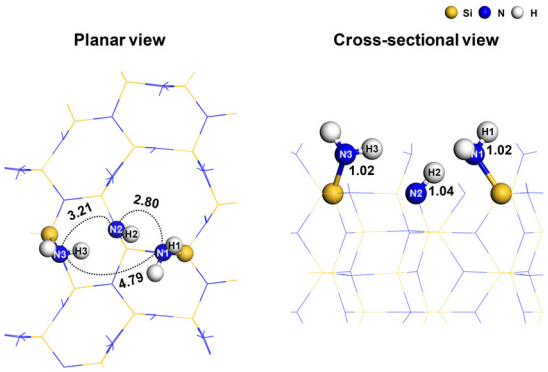

Fig. 1 The atomistic structure of the $-NH_2^*$ and –NH* terminated silicon nitride surface with the reaction sites. In the planar view, the dotted lines represent the interatomic distances with corresponding values in Å. In the cross-sectional view, the N–H bond lengths are shown in Å.

Computational methods

The DFT calculations were performed with the DMol^3 code in the Materials Studio 7.0 package[29,30] using the generalized gradient approximation (GGA) with the Perdew–Burke–Ernzerhof (PBE) functional.[31] The all-electron core treatment and the double numerical polarization (DNP) 4.4 basis set[29] with a global cutoff scheme at 4.6 Å were used for all calculations. The Brillouin zone integration was sampled within a 2 × 2 × 1 Monkhorst–Pack *k*-point mesh.[32] Dispersion force corrections based on the Grimme's method (DFT-D2)[33] were considered to account for long-range van der Waals (vdW) interactions. The convergence tolerance, self-consistent field (SCF), and thermal smearing parameters were the same as in previous reports.[25,34] Transition state (**TS**) was located using the complete linear-quadratic synchronous transit (LST-QST) or QST method with root mean square (RMS) force gradient criteria of 0.002 Ha/Å.[35] The **TS** needed to meet the additional criterion of having only one imaginary vibration mode, which was determined by frequency calculation. Further details of the TS search have been reported elsewhere.[34]

For this study, we chose the β-Si_3N_4 (001) surface that was fully passivated with 12 $SiNH_2^*$ and 12 NH*. This surface was also used in the previous reaction mechanism studies.[25,36,37] The surface had cell parameters of $a = b = 15.320$ Å. The slab model consisted of a four-layer (2 × 2) supercell with 184 atoms (48 silicon, 76 nitrogen, and 60 hydrogen atoms). The surface contained evenly distributed $-NH_2^*$ and –NH* sites, with a density of 5.89 per nm^2 each. The surface construction is described in detail in a previous work.[36] Fig. 1 shows the atomistic structure of the surface before the surface reaction of $SiCl_4$. The N–H bonds that undergo subsequent ligand exchange reactions are labeled N1–H1, N2–H2, and N3–H3, respectively. The $-NH_2^*$ sites are more sterically exposed to the precursor molecules than the –NH* sites, so we assumed that the first reaction would occur at $-NH_2^*$ (N1–H1). We also assumed that the second and third reactions would occur at neighboring –NH* (N2–H2) and $-NH_2^*$ (N3–H3) sites adjacent to N1–H1. The distances between the sites were 2.80 Å, 3.21 Å and 4.79 Å. The N–H bond length was 1.02 Å for $-NH_2^*$ and 1.04 Å for –NH*. The lower half of the slab model was constrained, while the upper half was relaxed. A 20 Å-thick layer of vacuum was inserted between the adjacent slabs to prevent interactions.

Several states were considered for the interaction of the precursor molecules on the surface, namely the unbound reactant state (**UR**), the reactant state ($\mathbf{R}_n$), and the product state ($\mathbf{P}_n$). **UR** is the state in which the precursor does not interact with the surface, assuming it is at an infinite distance from the surface. **R1** is the state where the precursor physisorbs on the surface. **P1**, **P2**, and **P3** are the product states with first, second, and third Si–N bonds, respectively. **R2** and **R3** are the reactant states after removing a byproduct molecule to infinity from **P1** and **P2**, respectively. **TS1**, **TS2**, and **TS3** are the transition states between the reactant and product states. All the structures used in this work can be found as ESI† in XYZ file format. The adsorption energy (E_{ads}), reaction energy (ΔE_n), activation energy (E_{An}), and desorption energy ($E_{des,n}$) of the *n*th reaction (n = 1–3) are defined as follows:

$$E_{ads} = E_R - (E_{surface} + E_{precursor}) \quad (1)$$

$$\Delta E_n = E_{Pn} - E_{Rn} \quad (2)$$

$$E_{An} = E_{TSn} - E_{Rn} \quad (3)$$

$$E_{des,n} = (E_{Reacted\ surface} + E_{byproduct}) - E_{Pn} \quad (4)$$

where E_{Rn} and E_{Pn} are the total system energies of the reactant and product states. E_{TSn} is the total energy of the transition state. $E_{surface}$, $E_{precursor}$, and $E_{byproduct}$ are the energies of the surface only, a precursor molecule and a byproduct molecule, respectively. $E_{Reacted\ surface}$ is the energy of the surfaces after the desorption of the byproduct molecules.

To study the desorption of the byproduct as a function of temperature, the free energies were determined by DFT using the following equation:

$$\Delta G = \Delta G^\circ + RT \ln p_{byproduct} \quad (5)$$

where ΔG° is the standard free energy at 1 atm, R is the ideal gas constant (8.63×10^{-5} eV mol^{-1} K^{-1}), T is the temperature in K, and $p_{byproduct}$ is the partial pressure of the byproduct in atm.

The partial pressure was assumed to be 1 Torr. ΔG° was estimated using the following equation:

$$\Delta G^{\circ} = (E_{\mathrm{des},n} + \Delta \mathrm{ZPE} + \Delta E_{\mathrm{v}}(T) + \Delta E_{\mathrm{r}}(T) + \Delta E_{\mathrm{t}}(T) + RT) - T\Delta S(T) \quad (6)$$

where ΔZPE, $\Delta E_{\mathrm{v}}(T)$, $\Delta E_{\mathrm{r}}(T)$, $\Delta E_{\mathrm{t}}(T)$, and $\Delta S(T)$, represent the difference between $\mathbf{R}_{n+1}$ and $\mathbf{P}_n$ states at temperature T (in K) in zero point energy, vibrational energy, rotational energy, translational energy, and entropy, respectively.

Results and discussion

During the initial reaction of the silicon precursor with the β-Si_3N_4 (001) surface, the $SiNH_2^*$ surface site is not only more sterically exposed but also more reactive than NH*, as discussed in the previous study.[25] Based on the electronegativity of Si (1.90) and Cl (3.16) atoms in $SiCl_4$ and N (3.04) and H (2.20) atoms of the surface $-NH_2^*$ site,[38] Si and Cl atoms are expected to interact with N and H atoms, respectively. Therefore, the two types of pathways, HCl byproduct formation (denoted as **P1a**) and $NH_3^+Cl^-$ complex formation (denoted as **P1b**), were modeled and simulated from the physisorption state (denoted as **R1**) as described in the following reaction equations:

$$-\mathrm{Si}-\mathrm{NH}_2^* + \mathrm{SiCl}_4 \rightarrow -\mathrm{Si}-\mathrm{NH}-\mathrm{SiCl}_3^* + \mathrm{HCl} \quad (7)$$

$$-\mathrm{Si}-\mathrm{NH}_2^* + \mathrm{SiCl}_4 + -\mathrm{Si}-\mathrm{NH}_2^* \rightarrow -\mathrm{Si}-\mathrm{NH}-\mathrm{SiCl}_3^* + -\mathrm{Si}-\mathrm{NH}_3^+\mathrm{Cl}^{-*} \quad (8)$$

Fig. 2 shows the reaction schemes from **R1** to **P1a** or **P1b**, along with the corresponding reaction and activation energy values. Both pathways were exothermic. However, the formation of **P1a** was less exothermic (−0.73 eV) than that of **P1b** (−1.31 eV). The reaction energy of **P1a** was mainly due to the formation of Si–N (4.82 eV) and H–Cl (4.53 eV) bonds despite the dissociation of N–H (4.57 eV) and Si–Cl (4.57 eV) bonds. The bond dissociation energies (BDE) were estimated using gas-phase models, as summarized in Fig. S1 (ESI†). The reaction energy of **P1b** could not be explained solely by the formation of Si–N and N–H (3.40 eV) bonds and the dissociation of N–H and Si–Cl bonds alone. The ionic interaction between NH_3^+ and Cl^- contributes to the reaction energy of **P1b**, making it more exothermic than **P1a**. Both **P1a** and **P1b** have similar activation energy values of 0.27 eV and 0.26 eV, respectively. The activation energy of 0.26 eV for **P1b** is similar to that of 0.3 eV reported for $NH_3^+Cl^-$ complex formation by DCS.[26] **P1b** was found to be more favorable than **P1a** due to its greater exothemicity when $SiCl_4$ initially interacted with the silicon nitride surface.

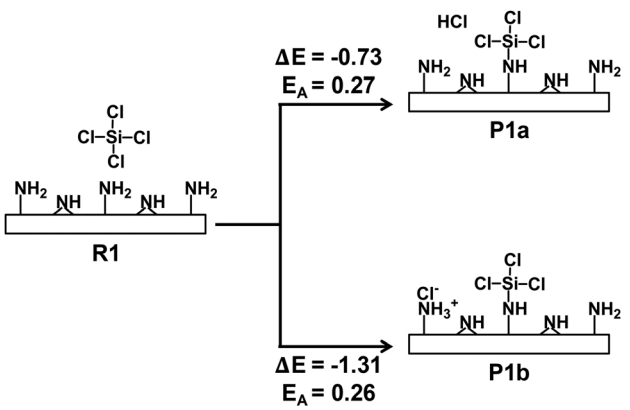

Fig. 2 The reactions scheme from the reactant state **R1** to the product states **P1a** and **P1b**. All energies are in eV.

Fig. 3 shows the changes in atomistic geometry during the initial reaction of $SiCl_4$. The other $-NH_2^*$ site shown in this figure is one of the neighboring sites to which the H atom will migrate in **P1b**, as shown in Fig. S2 (ESI†). In **TS1a** and **TS1b**, the Cl1 atom dissociated from $SiCl_4$, and the Si atom of $SiCl_4$ formed an elongated bond to the N1 atom with a distance of 1.83 Å. Additionally, the N1–H1 bond remained unbroken, resulting in a lower activation energy. The N1–H1 bond was elongated from 1.02 Å to 1.14 Å due to the overcoordination of the N1 atom. The strong interaction between the C11 and the surface H atoms also lowered the system energy. A similar transition state structure has also been reported.[27] In a previous work,[25] we obtained a transition state significantly different from **TS1b**. The Si–N1 bond was not formed, and H1 was dissociated from N1 to form the H1–Cl1 bond, resulting in a high activation energy of 4.49 eV.

The Mulliken atomic charges[39] were calculated and are presented in Table 1. In **R1**, the Si and Cl atoms in $SiCl_4$ have charges of 1.257 *e* and −0.349 *e*, respectively. For the surface $-NH_2^*$ site, the N1 and H1 atoms have charges of −0.864 *e* and 0.232 *e*, respectively. In **TS1a** and **TS1b**, the atomic charge of Si and N1 atoms increased due to the formation of an elongated Si–N1 bond. In **P1a** and **P1b**, the stable Si–N1 bond formation slightly increased the atomic charges of Si and N1 atoms. The charges of H1 and Cl1 atoms in HCl were similar in **P1a** with values of 0.285 *e* and −0.290 *e*, respectively. However, in **P1b**, the charge of the Cl1 atom significantly increased to −0.710 *e*, indicating a strong ionic interaction between Cl and $-NH_3^*$.

When HCl molecules were desorbed from the $NH_3^+Cl^-$ surface complex in **P1b**, the $-NH_2$ surface sites were restored, and the resulting surface became **R2**, the reactant state for the subsequent reaction. The energy required for the desorption of HCl molecules was calculated from eqn (4), and 1.29 eV was obtained. The free energy change due to the desorption of HCl molecules with temperature was also calculated from eqn (5), as shown in Fig. 4. A minimum temperature of 205 °C is required for HCl molecules to spontaneously desorb from the surface. Therefore, elevated temperature is a prerequisite for the recovery of the $-NH_2$* surface sites.

Fig. 5 shows the comprehensive energy diagram for the surface reaction of $SiCl_4$ on the silicon nitride surface. Only the pathway associated with $NH_3^+Cl^-$ complex formation was considered. For the first ligand exchange reaction, only the **P1b** pathway in Fig. 2 is shown as **P1** in Fig. 5. For the second and third reactions to form **P2** and **P3**, the reactions of $-SiCl_3^*$ with the N2–H2 site and $-SiCl_2^*$ with the N3–H3 site were assumed,

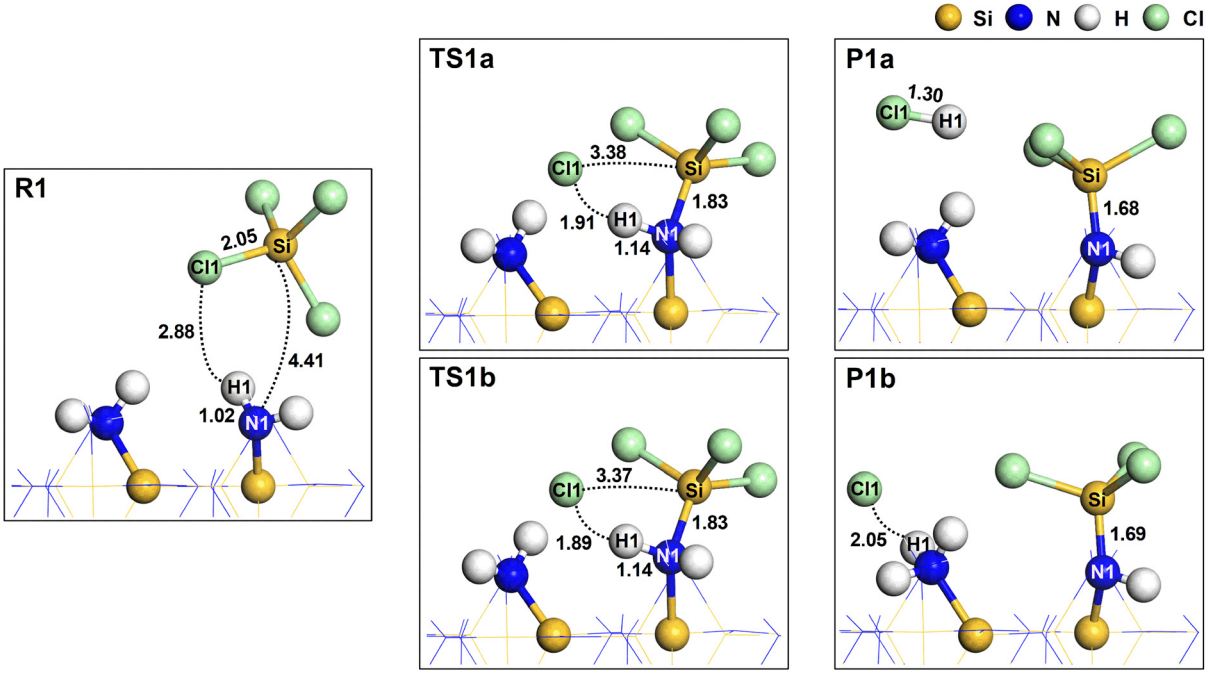

Fig. 3 The atomistic structures for the reactant (**R1**), transition (**TS1a** and **TS1b**), and product (**P1a** and **P1b**) states. The dotted lines represent the interatomic distances with corresponding values in Å. The bond lengths are also shown in Å.

Table 1 The Mulliken atomic charges for the reactant (**R1**), transition (**TS1a** and **TS1b**), and product (**P1a** and **P1b**) states

	Mulliken atomic charge (e)				
Atom	**R1**	**TS1a**	**TS1b**	**P1a**	**P1b**
Si	1.257	1.321	1.321	1.332	1.300
Cl	−0.349	−0.647	−0.647	−0.290	−0.710
N1	−0.864	−1.009	−1.009	−1.117	−1.134
H1	0.232	0.332	0.332	0.285	0.308

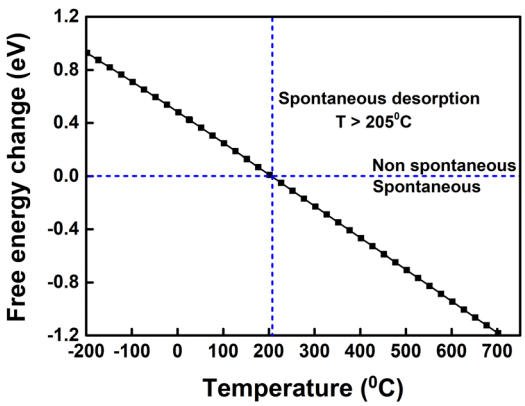

Fig. 4 The free energy change for the desorption of an HCl molecule from the $NH_3^+Cl^-$ surface site in **P1b** as a function of temperature.

as described in the following reaction equations:

$$-\mathrm{Si}-\mathrm{NH}-\mathrm{SiCl_3}^*+-\mathrm{NH}^*-+-\mathrm{Si}-\mathrm{NH_2}^* \rightarrow -\mathrm{Si}-\mathrm{NH}-\mathrm{SiCl_2}^*-\mathrm{N}-+-\mathrm{Si}-\mathrm{NH_3}^+\mathrm{Cl}^{-*} \quad (9)$$

$$-\mathrm{Si}-\mathrm{NH}-\mathrm{SiCl_2}^*-\mathrm{N}-+-\mathrm{Si}-\mathrm{NH_2}^*+-\mathrm{Si}-\mathrm{NH_2}^* \rightarrow -(\mathrm{Si}-\mathrm{NH})_2-\mathrm{SiCl}^*-\mathrm{NH}-+-\mathrm{Si}-\mathrm{NH_3}^+\mathrm{Cl}^{-*} \quad (10)$$

The reaction in eqn (9) was exothermic with an activation energy of 2.17 eV, while the reaction in eqn (10) was endothermic with an activation energy of 1.55 eV. The endothermic reaction and the higher activation energy indicate that the formation of **P3** is not favorable. Therefore, the chemisorbed species would be $-SiCl_2^*$ when the surface is exposed to $SiCl_4$.

Fig. 6 shows the atomistic structures of the **R2**, **TS2**, and **P2** states. The reaction energy was −0.30 eV, which is significantly less exothermic than **P1** because the subsurface bonds were elongated in **P2**, as shown in Fig. S3 (ESI†). In addition, the reaction in eqn (9) had a higher activation energy of 2.17 eV than 0.26 eV in eqn (8). In **TS2**, the Si–Cl2 and N2–H2 bonds were dissociated, and an elongated Si–N2 bond with a length of 1.81 Å was formed. The higher activation energy to form **P2** than **P1** was mainly due to the additional dissociation of the N2–H2 bond. The Mulliken atomic charges for **R2**, **TS2** and **P2** states are presented in Table S1 (ESI†). The trend remains consistent with the change from **R1** to **P1b**.

Similar to the desorption of HCl from **P1**, the desorption of the HCl molecule from **P2** was simulated. A desorption energy of 1.35 eV was obtained, similar to 1.29 eV for the **P1** case. The free energy change due to the desorption of HCl was estimated as a function of temperature, as shown in Fig. 7. A minimum of 276 °C would be required to restore the $-NH_2$ site to form **R3**, the reactant state for the subsequent reaction.

Fig. 8 shows the atomistic structures of **R3**, **TS3**, and **P3**. The reaction was endothermic with a reaction energy of 0.98 eV, in

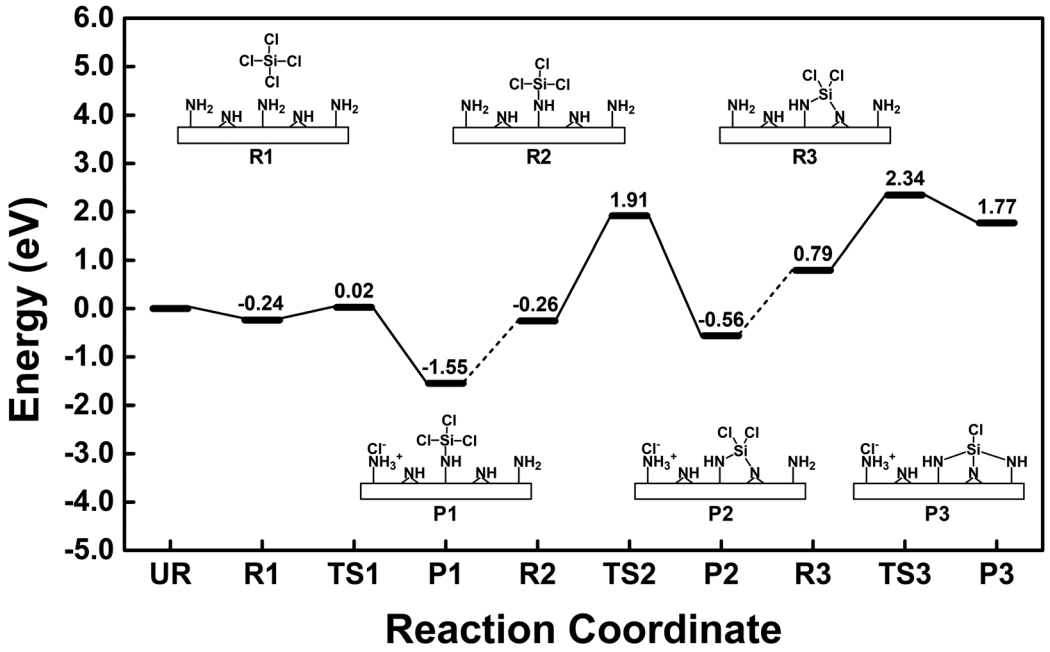

Fig. 5 Energy diagram for the chemisorption of $SiCl_4$ on silicon nitride.

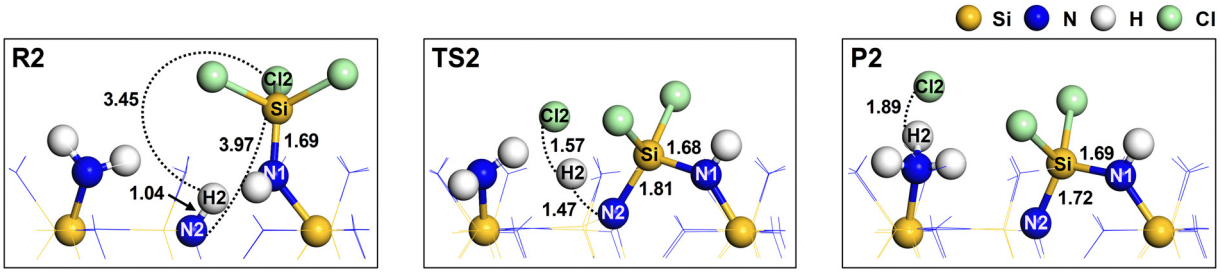

Fig. 6 The atomistic structures for the reactant (**R2**), transition (**TS2**), and product (**P2**) states of the second Si–N bond formation reaction. The dotted lines represent the interatomic distances with corresponding values displayed in Å. The bond lengths are also shown in Å.

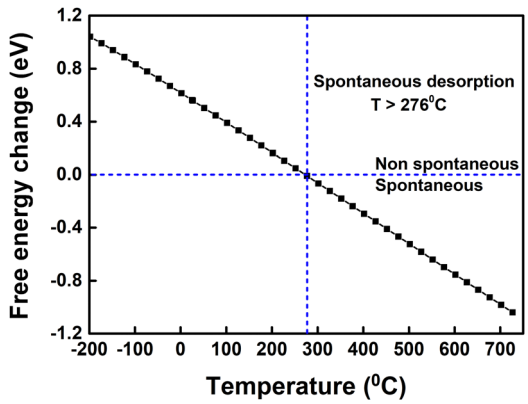

Fig. 7 The free energy change for the desorption of an HCl molecule from the $NH_3^+Cl^-$ surface site in **P2** as a function of the temperature.

contrast to the exothermicity of the previous reactions leading to **P1** and **P2**. The endothermic nature of the reaction leading to **P3** was mainly caused by the stretching of the Si–N1 and Si–N3 bonds, which were stretched to 1.79 Å in **P3**. In addition, the N–Si–N bond angles in **P3** were significantly distorted from the tetrahedral structure. The N1–Si–N2 bond angle was reduced from 108.6° in **R3** to 95.2° in **P3**. The angles of N1–Si–N3 and N2–Si–N3 were 146.8° and 97.0°, respectively. In **TS3**, the Si–Cl3 and N3–H3 bonds were dissociated, and elongated Si–N3 and H3–Cl3 bonds were formed with lengths of 1.87 Å and 1.48 Å, respectively. The lower activation energy for the formation of **P3** than **P2** was mainly due to the additional formation of the H3–Cl3 bond. The Mulliken atomic charges for **R3**, **TS3**, and **P3** states are presented in Table S2 (ESI†). The trend remains consistent with the change from **R1** to **P1b**.

The present work shows that the $NH_3^+Cl^-$ complex formation is significant for the chemisorption of $SiCl_4$. Our calculation is consistent with previous findings on the chemisorption of DCS on the surface of silicon nitride, where $NH_3^+Cl^-$ complex formation has been reported.[26,28] The $-NH_2^*$ reaction sites are restored by desorption of HCl from the $NH_3^+Cl^-$ complexes at elevated temperatures. NH_x surface groups have been reported for various nitride surfaces, including titanium nitride,[40] and boron nitride.[41] However, DFT

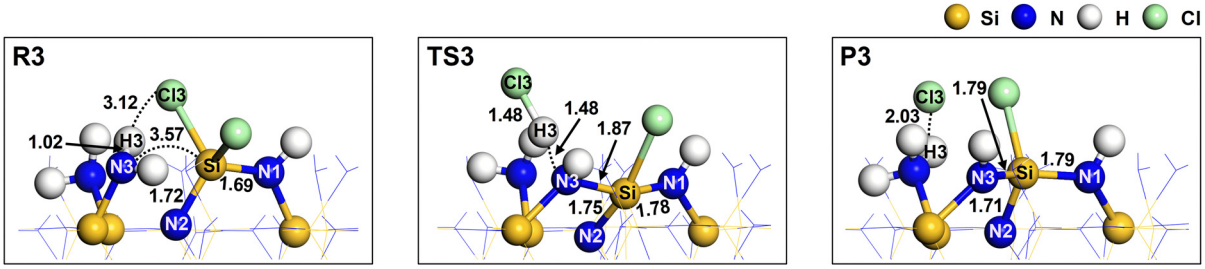

Fig. 8 The atomistic structures for the reactant (**R3**), transition (**TS3**), and product (**P3**) states of the third Si–N bond formation reaction. The dotted lines represent the interatomic distances with corresponding values displayed in Å. The bond lengths are also shown in Å.

studies on nitride surfaces have not considered the formation of $NH_3^+Cl^-$ but only HCl.[41,42] We hope that our work considering the $NH_3^+Cl^-$ complexes can be applied to the reaction mechanism studies of other nitride films using chloride precursors.

Conclusion

The chemisorption of $SiCl_4$ on the NH_2/NH-terminated silicon nitride surface was studied by DFT calculations using a slab model. The $NH_3^+Cl^-$ complex formation pathway was more exothermic than the HCl formation pathway, with a low activation energy of 0.26 eV. The $-NH_2^*$ reaction sites are restored by desorption of HCl from the $NH_3^+Cl^-$ complexes at elevated temperatures of 205 °C or higher. Three sequential ligand exchange reactions forming Si–N bonds on the silicon nitride surface were modeled and simulated. The reaction energies became progressively less exothermic as the reaction progressed due to the stretching of the Si–N bonds and the distortion of the N–Si–N bond angles in **P2** and **P3**. Also, the activation energies for the second and third reactions were significantly higher than that of the first reaction, mainly due to the additional dissociation of the N–H bond. The endothermic reaction and the higher activation energy indicate that the species would be $-SiCl_2^*$ when the surface is exposed to $SiCl_4$.

Author contributions

Tanzia Chowdhury: conceptualization, methodology, validation, formal analysis, investigation, writing – original draft, visualization. Khabib Khumaini: methodology, validation, formal analysis, investigation, writing – original draft, visualization. Romel Hidayat: methodology, validation, formal analysis, investigation, writing – review & editing. Hye-Lee Kim: methodology, validation, formal analysis, investigation, writing – review & editing. Won-Jun Lee: conceptualization, methodology, formal analysis, resources, writing – review & editing, supervision, project administration, funding acquisition.

Conflicts of interest

There are no conflicts to declare.

Acknowledgements

This work was supported by the Technology Innovation Program (Public-private joint investment semiconductor R&D program (K-CHIPS) to foster high-quality human resources) (RS-2023-00232222) funded by the Ministry of Trade, Industry & Energy (MOTIE, Korea) (1415187363). This research was also supported by the Korea Basic Science Institute (National Research Facilities and Equipment Center) grant funded by the Ministry of Education (2022R1A6C101A774).

References

1 F. Koehler, D. H. Triyoso, I. Hussain, S. Mutas and H. Bernhardt, *IOP Conf. Ser. Mater. Sci. Eng.*, 2012, **41**, 012006.
2 H. Kim, H. Song, C. Shin, K. Kim, W. Jang, H. Kim, S. Shin and H. Jeon, *J. Vac. Sci. Technol. A*, 2017, **35**, 01A101.
3 S. S. Kim, S. K. Yong, W. Kim, S. Kang, H. W. Park, K. J. Yoon, D. S. Sheen, S. Lee and C. S. Hwang, *Adv. Mater.*, 2022, **35**, 2200659.
4 R. A. Ovanesyan, E. A. Filatova, S. D. Elliott, D. M. Hausmann, D. C. Smith and S. Agarwal, *J. Vac. Sci. Technol., A*, 2019, **37**, 060904.
5 R. A. Ovanesyan, D. M. Hausmann and S. Agarwal, *ACS Appl. Mater. Interfaces*, 2015, **7**, 10806–10813.
6 S. Yokoyama, N. Ikeda, K. Kajikawa and Y. Nakashima, *Appl. Surf. Sci.*, 1998, **130–132**, 352–356.
7 H. C. M. Knoops, K. De Peuter and W. M. M. Kessels, *Appl. Phys. Lett.*, 2015, **107**, 014102.
8 N. Leick, J. M. M. Huijs, R. A. Ovanesyan, D. M. Hausmann and S. Agarwal, *Plasma Process. Polym.*, 2019, **16**, 1–7.
9 W. Jang, H. Jeon, C. Kang, H. Song, J. Park, H. Kim, H. Seo, M. Leskela and H. Jeon, *Phys. Status Solidi A*, 2014, **211**, 2166–2171.
10 J.-M. Park, S. J. Jang, L. L. Yusup, W.-J. Lee and S.-I. Lee, *ACS Appl. Mater. Interfaces*, 2016, **8**, 20865–20871.
11 J.-M. Park, S. J. Jang, S.-I. Lee and W.-J. Lee, *ACS Appl. Mater. Interfaces*, 2018, **10**, 9155–9163.
12 H. Cho, N. Lee, H. Choi, H. Park, C. Jung, S. Song, H. Yuk, Y. Kim, J.-W. Kim, K. Kim, Y. Choi, S. Park, Y. Kwon and H. Jeon, *Appl. Sci.*, 2019, **9**, 3531.
13 X. Meng, Y.-C. Byun, H. S. Kim, J. S. Lee, A. T. Lucero, L. Cheng and J. Kim, *Materials*, 2016, **9**, 1007.

14 J. W. Klaus, A. W. Ott, A. C. Dillon and S. M. George, *Surf. Sci.*, 1998, **418**, L14–L19.
15 W.-J. Lee, J.-H. Lee, C. O. Park, Y.-S. Lee, S.-J. Shin and S.-K. Rha, *J. Korean Phys. Soc.*, 2004, **45**, 1352–1355.
16 S. Morishita, S. Sugahara and M. Matsumura, *Appl. Surf. Sci.*, 1997, **112**, 198–204.
17 W.-J. Lee, U.-J. Kim, C.-H. Han, M.-H. Chun, S.-K. Rha and Y.-S. Lee, *J. Korean Phys. Soc.*, 2005, **47**, 598–602.
18 S. Riedel, J. Sundqvist and T. Gumprecht, *Thin Solid Films*, 2015, **577**, 114–118.
19 M. Edmonds, K. Sardashti, S. Wolf, E. Chagarov, M. Clemons, T. Kent, J. H. Park, K. Tang, P. C. McIntyre, N. Yoshida, L. Dong, R. Holmes, D. Alvarez and A. C. Kummel, *J. Chem. Phys.*, 2017, **146**, 0–12.
20 D. Sibanda, S. T. Oyinbo and T. C. Jen, *Nanotechnol. Rev.*, 2022, **11**, 1332–1363.
21 Y. Widjaja and C. B. Musgrave, *Phys. Rev. B*, 2001, **64**, 205303.
22 S. D. Elliott, G. Dey, Y. Maimaiti, H. Ablat, E. A. Filatova and G. N. Fomengia, *Adv. Mater.*, 2016, **28**, 5367–5380.
23 C. K. Ande, H. C. M. Knoops, K. De Peuter, M. Van Drunen, S. D. Elliott and W. M. M. Kessels, *J. Phys. Chem. Lett.*, 2015, **6**, 3610–3614.
24 L. Huang, B. Han, B. Han, A. Derecskei-Kovacs, M. Xiao, X. Lei, M. L. O'Neill, R. M. Pearlstein, H. Chandra and H. Cheng, *Phys. Chem. Chem. Phys.*, 2014, **16**, 18501–18512.
25 L. L. Yusup, J.-M. Park, T. R. Mayangsari, Y.-K. Kwon and W.-J. Lee, *Appl. Surf. Sci.*, 2018, **432**, 127–131.
26 G. Hartmann, P. L. G. Ventzek, T. Iwao, K. Ishibashi and G. S. Hwang, *Phys. Chem. Chem. Phys.*, 2018, **20**, 29152–29158.
27 N.-K. Yu, C. H. Moon, J. Park, H.-B.-R. Lee and B. Shong, *Appl. Surf. Sci.*, 2021, **565**, 150603.
28 T. Yang, E. S. Cheng, S. M. Johnson, T. Iwao, J. Zhao, J. G. Ekerdt, P. L. G. Ventzek and G. S. Hwang, *Appl. Surf. Sci.*, 2023, **629**, 157432.
29 B. Delley, *J. Chem. Phys.*, 1990, **92**, 508–517.
30 B. Delley, *J. Chem. Phys.*, 2000, **113**, 7756–7764.
31 J. P. Perdew, K. Burke and M. Ernzerhof, *Phys. Rev. Lett.*, 1996, **77**, 3865–3868.
32 H. J. Monkhorst and J. D. Pack, *Phys. Rev. B*, 1976, **13**, 5188.
33 S. Grimme, *J. Comput. Chem.*, 2006, **27**, 1787–1799.
34 K. Khumaini, R. Hidayat, T. R. Mayangsari, T. Chowdhury, H.-L. Kim, S.-I. Lee and W.-J. Lee, *Appl. Surf. Sci.*, 2022, **585**, 152750.
35 N. Govind, M. Petersen, G. Fitzgerald, D. King-Smith and J. Andzelm, *Comput. Mater. Sci.*, 2003, **28**, 250–258.
36 L. L. Yusup, J.-M. Park, Y. H. Noh, S. J. Kim, W.-J. Lee, S. Park and Y.-K. Kwon, *RSC Adv.*, 2016, **6**, 68515–68524.
37 T. Chowdhury, R. Hidayat, H.-L. Kim, T. R. Mayangsari, S. Cho, S. Park, J. Jung and W.-J. Lee, *Appl. Surf. Sci.*, 2021, **554**, 149481.
38 A. L. Allred, *J. Inorg. Nucl. Chem.*, 1961, **17**, 215–221.
39 R. S. Mulliken, *J. Chem. Phys.*, 1955, **23**, 2338–2342.
40 M. Q. Snyder, B. A. McCool, J. DiCarlo, C. P. Tripp and W. J. DeSisto, *Thin Solid Films*, 2006, **514**, 97–102.
41 N. Uene, T. Mabuchi, M. Zaitsu, Y. Jin, S. Yasuhara and T. Tokumasu, *Comput. Mater. Sci.*, 2023, **217**, 111919.
42 J. Park, N. K. Yu, D. Jang, E. Jung, H. Noh, J. Moon, D. Kil and B. Shong, *Coatings*, 2020, **10**, 712.